This chapter is based on

2 Human osteoblast-derived extracellular matrix with high homology to bone proteome is osteopromotive

Marta Baroncelli[1]*, Bram C.J van der Eerden[1], Siddharth Chatterji[1], Enrique Rull Trinidad[2], Yik Y. Kan[1], Marijke Koedam[1], Ingmar A.J van Hengel[3], Rodrigo D.A.M Alves[1], Lidy E. Fratila-Apachitei[3], Jeroen A.A Demmers[4], Jeroen van de Peppel[1], Johannes P.T.M van Leeuwen[1]

[1]Department of Internal Medicine, Erasmus University Medical Center, Wytemaweg 80, 3015 CN, Rotterdam, The Netherlands
[2]Department of Precision and Microsystems Engineering, Delft University of Technology (TU Delft), Mekelweg 2, 2628CD Delft, The Netherlands
[3]Department of Biomechanical Engineering, Delft University of Technology (TU Delft), Mekelweg 2, 2628CD Delft, The Netherlands
[4]Proteomics Center, Erasmus University Medical Center, Wytemaweg 80, 3015 CN, Rotterdam, The Netherlands

In press in Tissue Engineering Part A, (TEA-2017-0448-R2)

ABSTRACT

Efficient osteogenic differentiation of mesenchymal stem cells (MSCs) is crucial to accelerate bone formation. In this context, the use of extracellular matrix (ECM) as natural 3D-framework mimicking *in vivo* tissue architecture is of interest. The aim of this study was to generate a devitalized human osteogenic MSC-derived ECM and to investigate its impact on MSC osteogenic differentiation to improve MSC properties in bone regeneration. The devitalized ECM significantly enhanced MSC adhesion and proliferation. Osteogenic differentiation and mineralization of MSCs on the ECM was quicker than in standard conditions. The presence of ECM promoted *in vivo* bone formation by MSCs in a mouse model of ectopic-calcification. We analyzed the ECM composition by mass spectrometry, detecting 846 proteins. Of these, 473 proteins were shared with the human bone proteome we previously described, demonstrating high homology to an *in vivo* microenvironment. Bioinformatic analysis of the 846 proteins showed involvement in adhesion and osteogenic differentiation, confirming the ECM composition as key modulator of MSC behaviour. In addition to known ECM-components, proteomic analysis revealed novel ECM functions, which could improve culture conditions. In summary, this study provides a simplified method to obtain an *in vitro* MSC-derived ECM that enhances osteogenic differentiation and could be applied as natural biomaterial to accelerate bone regeneration.

Key words: Mesenchymal stromal cells; extracellular matrix; bone; bone tissue engineering

INTRODUCTION

Mesenchymal stromal cells (MSCs) are promising candidates for bone regeneration, because they can differentiate towards osteoblasts and secrete trophic factors that modulate target cells [1, 2]. MSCs are combined with biomaterials for bone-tissue-engineering applications, and have been proposed to reduce skeletal defects [3].

To accelerate bone regeneration, differentiation of MSCs into bone-forming cells is critical. *In vivo*, MSC-derived osteoblasts deposit the surrounding extracellular matrix (ECM) that is subsequently mineralized [4]. The most abundant protein of the ECM is collagen type 1 (COL1A1). Together with hydroxyapatite crystals, the ECM physically supports bone cells to regulate mineral deposition. Furthermore, the bone ECM is a very dynamic tissue that contains and actively regulates the availability of growth factors (GFs) and signaling factors, such as bone morphogenic proteins (BMPs), and influences the signal transduction of these molecules. As a result, the ECM modulates MSC behavior, such as cell adhesion, proliferation and commitment [5, 6]. The specific composition of bone ECM is essential in this role. This is because proteoglycans (PGs) and enzymes such as alkaline phosphatase (ALP) and matrix metalloproteases (MMPs), enrich the ECM composition, along with the non-collagenous proteins (NCPs), such as osteonectin (SPARC), osteocalcin (BGLAP), osteopontin (OPN) and matrix gla proteins (MGP), which regulate collagen-fiber mineralization and cell-matrix adhesion [5].

Recently, the ECM has become increasingly important as a natural 3D framework, that modulates cell behavior and mimics the *in vivo* tissue architecture [7, 8]. Strategies combining ECM-coated scaffolds and MSCs have been proposed to improve the supportive role of scaffolds in bone regeneration [9]. In this context, *in vitro* cell-secreted ECMs have been produced according to several decellularization methods, and represent a suitable alternative to decellularized matrices from tissues [10]. Cell-derived ECMs have been proposed for extensive *ex-vivo* expansion of MSCs, as they promote proliferation and maintain the multi-lineage differentiation potential of MSCs [11-13]. Interestingly, osteoblast-derived ECM enhances the osteogenesis of MSCs [14, 15]. Although known ECM components such as collagen, fibronectin (FN), laminin, perlecan, biglycan, decorin were detected in these MSC-derived ECMs, their full composition is still under investigation [12, 16-19]. Nevertheless, the specific protein composition of ECM mediates these effects via cell-matrix interactions; for instance, COL1A1 and vitronectin (VTN) promote osteogenesis, and FN influences MSC behavior [6, 20-22]. However key ECM bioactive regulators of MSC functions have not yet been identified. The full composition of the ECM is difficult to disentangle due to its complex structure.

The aim of this study was to generate a devitalized ECM from human osteoblast-differentiated MSCs and investigate its effect on the osteogenic differentiation of MSCs and bone formation *in vivo*. The protein composition of the ECM was investigated by mass spectrometry and compared to the human bone proteome [23], in order to gain insight into how the ECM modulates MSC behavior and whether it mimics the *in vivo* bone microenvironment.

MATERIALS AND METHODS

Culture and devitalization of MSCs

Human bone marrow-derived MSCs were obtained commercially (PT-2501, Lonza, Walkersville, MD, USA). MSCs from a single donor at passage 7 were cultured in 12-well plates (5128 cells/cm^2; Greiner bio-one, Frickenhausen, Germany) in alpha-Mem (10% fetal bovine serum (FBS), pH 7.5, phenol-red free, Gibco BRL, Life technologies). After 2 days of culture in non-differentiating conditions, MSCs were cultured in osteogenic conditions for 11 days (medium was supplemented with 100 nM dexamethasone and 10 mM β glycerophosphate; Sigma, St. Louis, MO, USA) to induce the osteogenic differentiation.

Before the onset of mineralization, MSCs were devitalized as represented in Figure 1A. Briefly, MSCs were washed twice with Phosphate Buffered Saline (PBS, Gibco BRL, Carlsbad, CA, USA), frozen at -80°C and then thawed at room temperature, without PBS, for 20 minutes each. These steps were repeated 3 times and followed by a DNase I treatment for 30 minutes at 37°C (10 U/ml; Sigma-Aldrich, St Louis MO, USA). The devitalized matrix was gently rinsed 3 times with PBS, air dried in the culture-hood and stored at -20°C for at least 7 days before further experiments.

ECM characterization

The devitalized ECM was cultured in osteogenic medium for 6, 24 and 48 hours and the metabolic activity of the devitalized ECM was assessed by a viability indicator (Presto Blue® Cell Viability Agent, Life Technologies) following manufacturer's instructions. Fluorescence was measured by a microplate reader (Victor X4™ Multimode Plate Reader, Perkin Elmer; excitation 530nm, emission 590nm). Live MSCs cultured in osteogenic conditions were used as positive control.

The absence of cells after the devitalization treatment was demonstrated by 4,6-diamidino-2-phenylindole (DAPI) nuclear staining (Sigma Aldrich, St. Louis, MO, USA). MSCs cultured on plastic and on ECM for 24 hours were used as positive control.

To measure the roughness, the matrix was produced on glass-coverslips coated with Poly-L-Lysine (PLL) (St. Louis, MO, USA), following the devitalization procedure. Briefly, sterile glass-coverslips had been coated with PLL for 10 minutes and washed 3 times with milliQ water before cell-seeding. For the background measurements, the same treatment was applied to a coated coverslip without cells. A dynamic mode atomic force microscopy (AFM; NaniteAFM, Nanosurf GmbH, Germany) was used to measure the roughness of the ECM. Areas of 50 µm x 50 µm, 20 µm x 20 µm and 5 µm x 5 µm were scanned in 2 different areas of the matrix-surface with NCLR probes (non-contact long cantilever reflex coating, Nanoworld AG, Switzerland). Images of 20 µm x 20 µm scanned-areas were analyzed using Gwiddion (www.gwiddion.net). We quantified the roughness by drawing 8 lines across each image and considering the amplitude of Roughness Average (Ra) for each line, which is defined as the average deviation of all points of roughness profile from a mean line over the evaluation length. The Ra values of all the lines were eventually averaged to the final values. Measurements were representative of 2 independent experiments.

The surface of the devitalized ECM was imaged by scanning electron microscopy (SEM) using a JEOL JSM-IT100LA equipment (JEOL Europe BV, Nieuw-Vennep, The Netherlands). Samples were prepared as previously described [24]. Briefly, devitalized ECM on PLL-coated coverslip was washed with PBS, fixed (4% paraformaldehyde, 1% glutaraldehyde in PBS, pH 7.4), rinsed in demineralized water, dehydrated sequentially in graded alcohols (50% for 15 minutes, 70% for 20 minutes, 96% for 20 minutes), air dried and gold-coated. Different areas of 2 replicates were examined at various magnifications.

Cell adhesion analysis

In order to visualize the cell morphology and analyze the cell adhesion to the ECM by immunohistochemistry, the devitalized ECM was produced on polystyrene plastic. Next, MSCs in osteogenic conditions were cultured for 2, 4, and 8 hours. Actin-cytoskeleton was stained by rhodamine-conjugated phalloidin (Thermo Fisher Scientific); focal adhesions were visualized by staining vinculin (Vinculin Abfinity™ recombinant rabbit monoclonal antibody, Clone 42H89L44, Life Technology, USA; as secondary antibody: FITC goat-anti-rabbit IgG, BD Pharmigen) and visualized by a fluorescent microscope (Zeiss Axiovert 200 MOT microscope). Images with a magnification of 630X were considered and processed with Image J (www.imagej.nih.gov/ij, version 1.47n), as previously described [25]. Briefly, the background was subtracted by using the Sliding Paraboloid option, the local contrast enhanced by running the Clahe option, the Mathematical Subtract Function with a value of 10000 was applied to subtract the background, followed by Mathematical Exponential (EXP) to further minimize the background. The contrast was adjusted using Bright-

ness & Contrast tool. The number of focal adhesions relative to the area stained by phalloidin was quantified by Cell Profiler (www.cellprofiler.com, version 2.1.1). For the analysis, an average of 4 pictures with a magnification of 400x were considered, following the same steps as previously described with Image J, and analyzed using a self-made pipeline in Cell-Profiler.

The morphology of cells cultured on the devitalized ECM and in standard culture conditions on PLL-coated coverslips was observed by SEM. Cells were cultured in osteogenic conditions for 24 hours and processed as previously described [24] for the devitalized ECM. Images were acquired at various magnifications using secondary and backscattered imaging modes.

Cell-adhesion was quantified by Flow Cytometry (Accuri C6 Flow Cytometer, BD Biosciences, San Jose, CA, USA), using counting beads (Liquid Counting Beads, BD Biosciences, San Jose, CA, USA). MSCs in osteogenic conditions were cultured for 6 and 24 hours on ECM and plastic; after washing and trypsinization, the number of cells relative to a known concentration of fluorescent counting beads was counted. The result is representative of 3 independent experiments.

The heterogeneous MSC population was sorted based on ALP expression by Fluorescence-activated cell sorting (FACS) (FACS Jazz, BD Bioscience) (ALP antibody: PE mouse anti-human Alkaline Phosphatase, clone B4-78, BD Biosciences, San Jose, CA, USA). ALP-positive and ALP-negative sorted cells were seeded on the devitalized ECM in osteogenic medium, and cell-adhesion was measured after 24 hours of culture as previously described. Unsorted MSCs were used as control. Measurements were representative of 2 independent FACS-sorting experiments.

Cell proliferation analysis

For the measurement of proliferation, MSCs were cultured in osteogenic conditions on ECM and plastic dishes for 1, 3, and 5 days, and the percentage of Ki-67 positive cells was detected (Alexa Fluor 488 mouse anti-human Ki-67, BD Pharmigen) by Flow Cytometry (Accuri C6 Flow Cytometer, BD Biosciences, San Jose, CA, USA), within the Propidium Iodide-positive population (PI solution, BD Biosciences, San Jose, CA, USA). The result is representative of 3 independent experiments.

Culture of MSCs on ECM and analysis of osteogenic differentiation

Alkaline phosphatase activity and ECM mineralization were measured in cell-extracts of MSCs cultured in osteogenic conditions on ECM and plastic dishes for 19 days as previously described [26]. Mineralization was further confirmed by Alizarin red staining (ARS) [26]. The result is representative of 3 independent experiments.

In vivo ectopic bone formation analysis

In order to check whether the ECM would promote *in vivo* ectopic bone formation by MSCs, MSCs on hydroxyapatite and tricalcium phosphate beta (HA-TCP) with and without ECM have been subcutaneously implanted in immunocompromised mice (Non-obese diabetic/Scid IL2R gamma (NSG), Charles River Laboratories). ECM was produced and devitalized on 20 mg of HA-TCP (Triosite™, Zimmer Biomet, Warsaw, IN, USA) powder, following the same devitalization procedure as previously described. HA-TCPs were loaded with MSCs ($0.5x10^6$/ HA-TCP-pellet) in growth medium, let them attach overnight and subcutaneously implanted into 4 dorsal pockets in NSG mice (N=3) (10 weeks old, females and males) under anesthesia, as previously described [27]. ECM on HA-TCP and HA-TCP vehicle were used as controls. A schematic overview is presented in Figure 4A. Three independent experiments with similar sample size were performed. All animal procedures were approved by the Committee on the Ethics of Animal Experiments of Erasmus University Medical Center, Rotterdam, The Netherlands. Mice were kept in pathogen free facility (SPF), with 12-hours light/dark cycle, controlled temperature (22 ± 1 °C) and humidity (50 ± 5%), and fed *ad libitum* with standard rodent diet. All pellets were retrieved 8 weeks after implantation and ectopic calcification checked by Masson-Goldner staining. Briefly, pellets were fixed in 70% Ethanol, dehydrated in graded alcohols, plastic-embedded (Methyl methacrylate MMA) and cut into 6-µm-thick sections by microtome (RM2255, Leica Biosystem). Two stained sections of each pellet (1 from the periphery of the pellet and 1 from the core) were scanned by Nanozoomer 2.0 HT (Hamamatsu Photonics), and areas of newly formed mineralized bone over HA-TCP quantified by Image J (www.imagej.nih.gov/ij, version 1.47n), by 2 independent observers blind towards the data (as represented in Supplementary Figure 1A-C).

Mass spectrometry analysis

The proteomic composition of ECM was analyzed by mass spectrometry (MS), with a label-free quantification (LFQ) method. ECM samples were scraped and collected in 0.5ml of PBS Triton 0.1% and concentrated by using centrifugal filters (Amicon Utra-0.5 ml centrifugal filters, Millipore; 3KDa cutoff), following manufacturer's instructions. Protein content was quantified by BCA kit (Pierce Biotechnology, Rockford, IL, USA), following manufacturer's instruction. Protein extracts (2.5 µg) were reduced by NuPAGE® Reducing Agent and resolved by one-dimensional SDS-Page gel, in duplicate (NuPAGE®Novex® 4-12% Bis-Tris-Acetate Gels, Life technologies). Protein bands were stained with Coomassie staining (Bio-safe Coomassie, Bio-Rad, Hercules, CA, USA) for 1 hour and de-stained in milliQ water overnight. Samples were processed as previously described [28]. Briefly, an automatic gel slicer was used to cut gel lanes into 2-mm slices, that were subsequently in-gel reduced with

dithiothreitol, alkylated with iodoacetamide and digested with trypsin (Promega, sequencing grade, Madison, WI, USA). A 1100 series capillary LC system (Agilent Technologies) coupled to an LTQ-Orbitrap XL mass spectrometer (Thermo Scientific) was used in positive mode to perform Nanoflow LC-MS/MS. ReproSil C18 reversed phase column (Dr Maisch GmbH; 1.5 cm × 100 µm, packed in-house) were used to trap the peptide mixtures at a flow rate of 8 µl/min. Peptides were separated by a linear gradient from 0 to 80 % B (A = 0.1 % formic acid; B = 80% (v/v) acetonitrile, 0.1 % formic acid) in 170 minutes, at a constant flow rate of 200 nl/min, using a splitter, on ReproSil C18 reversed phase column (Dr. Maisch GmbH, Ammerbuch-Entringen, GE; 15 cm × 50 µm, packed in-house). The eluent was directly sprayed from the column into the ESI source of the mass spectrometer. Peptides were fragmented in data-dependent mode, and mass spectra acquired in continuum mode. The mass spectrometry proteomics data have been deposited to the ProteomeXchange Consortium via the PRIDE [29] partner repository with the dataset identifier PXD006865 (Username: reviewer20352@ebi.ac.uk; Password: LC3okFPV).

Bioinformatic analysis

The MaxQuant Software (version 1.5.0.0) was used to analyze the raw MS data, with a false discovery rate of 0.01 for proteins and peptides and 6 amino acids as minimum peptide length. The MS/MS spectra were searched by Andromeda search engine, against the human proteome as provided by Uniprot database (taxonomy: *Homo sapiens*, release HUMAN_2013_04) (uniprot.org, v2014_05), with the reversed versions of all the sequences (maximum of two missed cleavages; 0.6 Da fragment mass tolerance, enzyme specificity: trypsin). Samples were run in duplicates and then averaged for the analysis. LFQ values higher than zero were considered for the analysis. Over-represented Gene Ontology (GO) terms were analyzed by using DAVID Bioinformatic Resources v6.7 [30], using the whole human genome as background. Only significantly enriched terms (Benjamini P <0.01) were considered.

The protein composition of the devitalized ECM was compared to the one of 3 human bone samples that we previously described [23]. The shared proteins between the 2 data sets were analyzed through QIAGEN's Ingenuity® Pathway Analysis (IPA®, QIAGEN Redwood City www.qiagen.com/ingenuity).

Immunoblot analysis

The presence of some proteins detected by MS in the ECM was confirmed by Western blot. Briefly, ECM samples (12 µg) were prepared as for MS analysis, mixed with 6X reducing sample buffer, separated by SDS-PAGE and transferred onto nitrocellulose membrane (Hybond-ECL, Amersham Bioscience, Buckinghamshire, UK). After non-specific blocking with 5% BSA in Tris-buffered saline (TBS) 0.1% Tween-20,

membranes were incubated overnight with primary antibody against FN1 (mouse monoclonal to FN1, 1:5000, Ab-11, Clone FBN11, Termo Fisher Scientific, Rockford, IL, USA), ALP (mouse monoclonal to ALP, 1:1000, Clone 0.G.2, Abcam, Cambridge, UK), ANXA2 (rabbit polyclonal, 1:1000, Abcam, Cambridge, UK) and GAPDH loading control, mouse monoclonal, 1:1000, Clone sc-69778, Santa Cruz Biotechnology, Dallas, TX, USA). Membranes were probed with secondary antibody conjugated with goat-anti-mouse-Alexa Fluor 680 (goat-anti-mouse, 1:300, Invitrogen, Waltham, MA, USA) and IRDye 800CW (goat-anti-rabbit, 1:5000, LI-COR, Lincoln, NE, USA). Bands were visualized using the LI-COR Infrared Imaging System (LI-COR, Lincoln, NE, USA) according to manufacturer's instruction.

Statistical analysis

Data were representative of multiple independent experiments. All values were presented as average ± standard deviation (SD) of biological replicates, and significance was calculated by 2-way analysis of variance (ANOVA), followed by Bonferroni Post Hoc test, otherwise indicated elsewhere.

RESULTS

Preparation of MSC-derived ECM

To study the impact of the ECM on MSC behavior, we successfully produced an *in vitro* model of devitalized ECM by using freeze/thaw cycling as decellularization technique. As schematically represented in Figure 1A, MSCs were osteogenically differentiated to allow the production of the extracellular matrix, and before the onset of mineralization, devitalized by freeze/thaw cycles, followed by a DNAse treatment. Extensive washings were intended to withdraw the potential remaining live cells and the cellular debris. Taking advantage of an adaptation of a previous protocol [31], this devitalization procedure represented a simplified way of producing an *in vitro* cell-secreted ECM.

The ECM was metabolic inactive after the devitalization treatment and exhibited a rough surface

As the devitalization treatment should remove cells to minimize immune response, while maintaining the bioactivity of the matrix [9], we checked the efficacy of the devitalization treatment by using Presto Blue. Figure 1B illustrates that the devitalization treatment completely abolished the viability of the cells. In fact, while the metabolic activity of live MSCs increased over time as expected, the matrix remained metabolically inactive. DAPI nuclear staining showed that cells were absent after

devitalization treatment (Supplementary Figure 1D). This confirmed the validity of the devitalization treatment used to prepare the MSC-derived ECM.

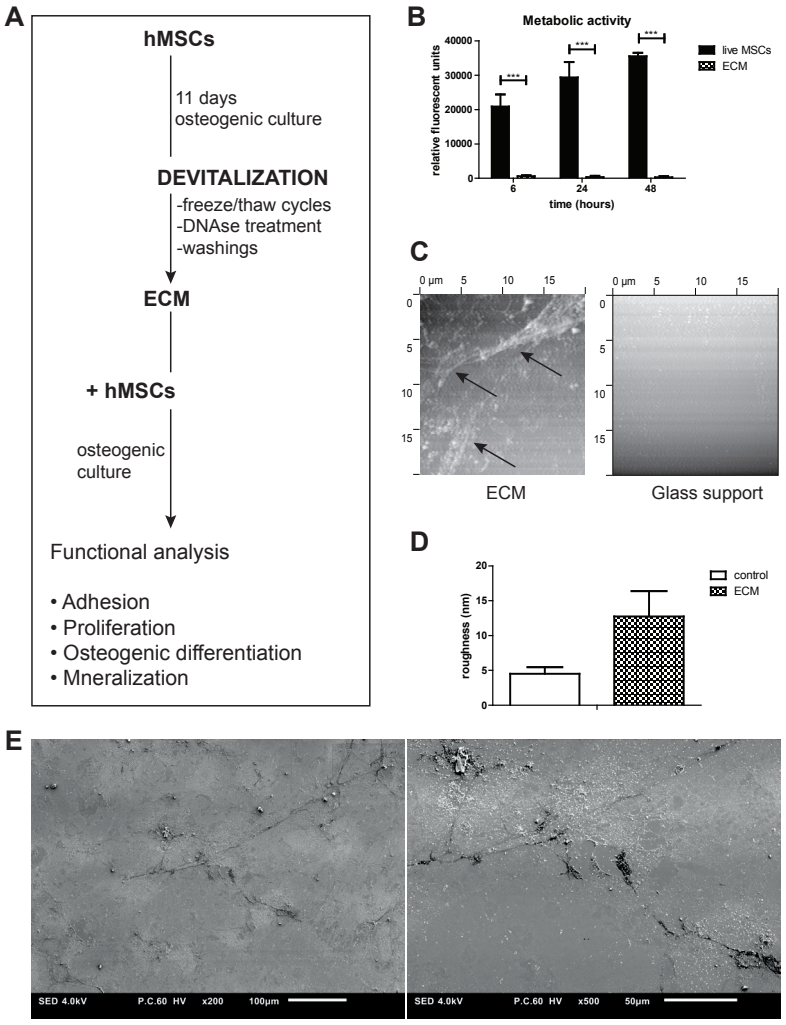

Figure 1. Preparation and characterization of MSC-derived ECM. A) Schematic overview of ECM-preparation and culture conditions. B) Metabolic activity of ECM and live MSCs measured at 6, 24 and 48 hours after seeding with Presto Blue viability agent. Values are presented as relative to blank (osteogenic medium with Presto Blue) (***, $P<0.001$) (N=3). C) AFM images of ECM and control (20 µm x 20 µm scans) on a glass substrate. Images represent the topography of the area analyzed, coming from the oscillation of the cantilever over the scanned surface. Black arrows indicate fiber-like structures. D) Roughness quantification of ECM and control, based on amplitude of average Roughness (Ra) values from independent scans. Values: Average ± SD. E) Scanning electron micrographs of the surface of devitalized ECM at 200X (left) and 500X magnification (right). Images are representative for multiple areas in 2 specimens. Scale bars indicate 100 µm (left) and 50 µm (right).

Next, we analyzed the surface of the devitalized ECM by atomic force microscopy. AFM images of the scanned areas showed that the matrix had a rough surface, and exhibited fiber-like structures relative to the featureless poly-L-lysine-coated surfaces (Figure 1C). Quantified data revealed a roughness of 12.75 nm for the ECM compared to 4.53 nm for the poly-L-lysine-coated surface without cells, as shown in Figures 1C and 1D. Investigations of larger areas of devitalized ECM by SEM confirmed the rough surface and the presence of fibrous structures and aggregates (Figure 1E).

The ECM increased MSC adhesion

Next, we investigated whether the devitalized ECM could enhance cellular attachment. Therefore, we analyzed the effect of the devitalized ECM on the adhesion of freshly seeded human MSCs. Figure 2A illustrates that MSCs adhere more efficiently and quicker on the devitalized ECM than on plastic. Within 2 hours after seeding the cells, the actin cytoskeleton was correctly organized to shape a proper morphology, as shown by phalloidin staining, whereas this was not yet the case for the MSCs seeded on plastic. In addition, vinculin staining showed that MSCs on ECM formed focal adhesions within 2 hours after seeding. At this time point, the number of focal adhesions per area stained by phalloidin in cells on ECM was more than 18-fold higher than in cells seeded on plastic. Although not significant, the number of focal adhesions was overall higher at each time point (Supplementary Figure 1E). These analyses illustrate that seeding cells on a preformed ECM significantly accelerates MSC adhesion. MSCs cultured for 24 hours on the devitalized ECM and in standard culture conditions exhibited a stretched morphology with focal adhesion complexes, but no substantial differences in morphology were highlighted when imaged at high magnification by SEM (Figure 2B). However, an increased number of cells were generally observed on the devitalized ECM relative to the standard culture conditions.

The increased cell adhesion was further confirmed by counting the number of the cells that adhere to the different substrates. Six hours after seeding on the ECM, the number of cells was 1.2-fold ($P<0.01$) higher than on plastic, and 1.3-fold ($P<0.05$) higher after 24 hours (Figure 2C).

In addition, we investigated the preferential adhesion of MSC subsets to the devitalized ECM. We focused on ALP-positive MSCs, considered as already osteogenic committed MSCs, and ALP-negative MSCs, considered as yet uncommitted MSCs. Hereto we FACS-sorted the heterogeneous population of MSCs based on ALP expression, and next seeded the ALP-positive and ALP-negative population on the devitalized ECM. After 24 hours of culture, no significant difference was detected in the adhesion of these subsets and the unsorted population (Figure 2D). The devitalized ECM was able to bind not only the committed ALP-positive MSCs, but also the ALP-negative cells.

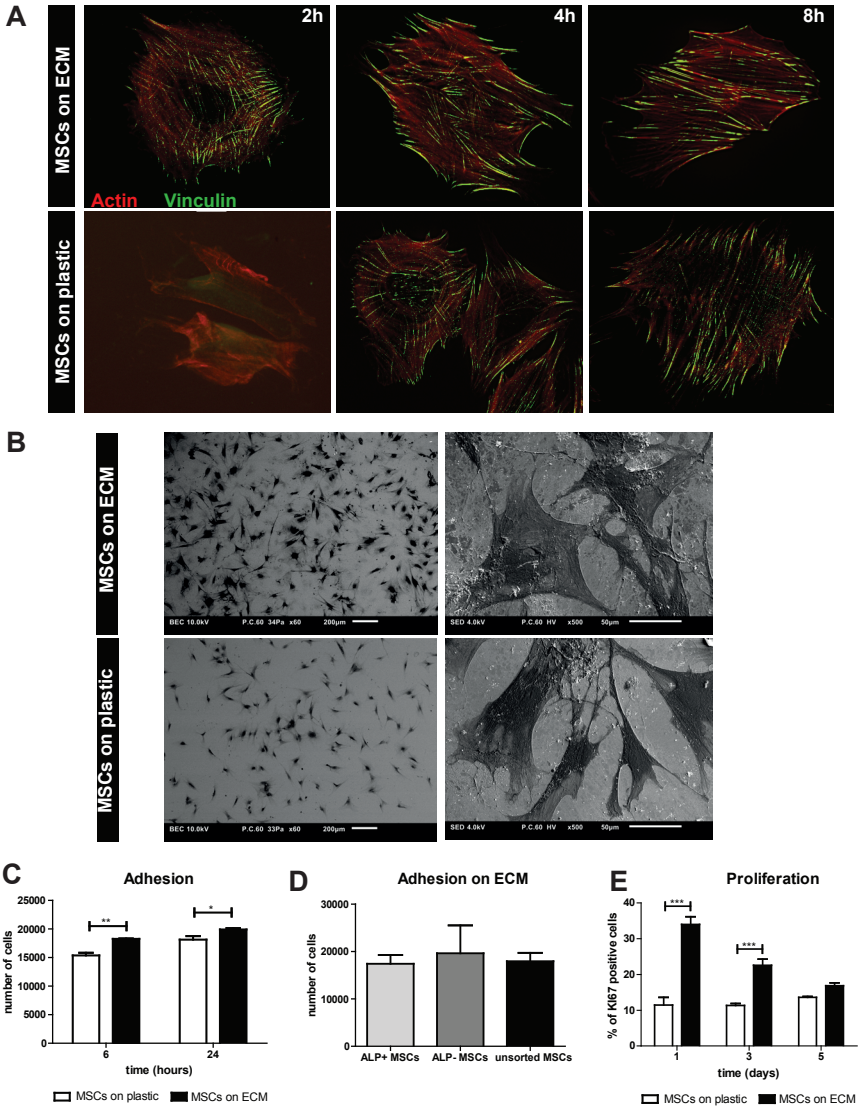

Figure 2. ECM enhances MSC adhesion and proliferation. A) Immunohistochemistry of MSCs on ECM (top) and plastic (bottom) at 2, 4, 8 hours after seeding. Red, phalloidin for actin cytoskeleton; green, vinculin of focal adhesions. B) SEM images of MSCs cultured on the devitalized ECM (top) and in standard culture conditions (bottom) for 24 hours, at 60X (left) and 500X magnification (right). Images are representative of multiple areas in 2 specimens. Scale bars indicate 200 μm (left) and 50 μm (right). C) Quantification of cells in adhesion to substrates counted by flow cytometry. D) Quantification of MSC subsets (ALP positive-, ALP negative-sorted cells, unsorted cells) in adhesion to the ECM for 24 hours, counted by flow cytometry (no significant difference was detected by One-way analysis of variance, followed by Bonferroni's Multiple Comparison Test). (ALP+ MSCs: ALP-positive sorted MSCs; ALP- MSCs: ALP-negative sorted MSCs). E) Proliferation of MSCs on ECM and on plastic as percentage of Ki-67 positive cells by flow cytometry. Results are representative of multiple independent experiments. (*, $P<0.05$; **, $P<0.01$; ***, $P<0.001$). Values: Average ± SD.

The ECM increased MSC proliferation and accelerated MSC osteogenic differentiation and mineralization *in vitro*

We investigated whether the accelerated attachment to the devitalized ECM was accompanied by an effect on cell proliferation, by analyzing the percentage of Ki-67 positive cells by flow cytometry. After 1 day of culture of MSCs on ECM, 34% of the cells were Ki-67 positive, whereas only 11% of the cells were positive when cultured on plastic. This illustrates that 24 hours of culture on ECM were sufficient to increase the number of proliferating MSCs by 2.97-fold (Figure 2E). The percentage of Ki-67 positive cells gradually decreased in time to similar levels as the cells seeded on plastic. After 5 days of osteogenic differentiation, the percentage of proliferating cells lowered to 16%.

Next, the influence of the ECM on the osteogenic differentiation of MSCs was studied. MSCs cultured on ECM differentiated faster toward osteoblasts than those grown on plastic. After 11 days of differentiation, ALP activity in MSCs cultured on ECM was 2.2-fold higher than their counterpart on plastic (Figure 3A). Furthermore, mineralization was accelerated and increased by culturing MSCs on the ECM, as illustrated by calcium deposition in the well and the alizarin red staining (Figures 3B-D). The amount of calcium deposited after 19 days of culture, as measure of mineralization, was more than 20-fold higher in MSCs cultured on ECM than on plastic (Figure 3B). Alizarin Red staining of the mineralized ECM confirmed the increased mineralization of cells seeded on devitalized ECM, as shown in Figures 3C and 3D.

ECM promoted *in vivo* ectopic bone formation by MSCs

Based on the osteopromotive role of the ECM on MSCs *in vitro*, we investigated whether the ECM influenced the *in vivo* bone formation by MSCs in an ectopic calcification model. MSCs with and without ECM were subcutaneously implanted on HA-TCP in immunocompromised mice and bone formation checked by Masson-Goldner staining after 8 weeks, as represented in Figure 4A. Histological evaluation showed that MSCs on HA in this experimental set-up induced ectopic bone formation (Figure 4B and C). In 2 out of 3 experiments MSCs implanted with ECM gave rise to about 20-fold higher amount of bone than when ECM was not present (Figure 4D). In the experiment that did not show an effect of ECM, the bone formation in control HA-TCP was already at the level induced by the ECM conditions in the other experiments, potentially explaining that an additional increase was not observed. Overall, in contrast to the control condition, the presence of ECM robustly led to ectopic bone formation in all experiments (Figure 4D). Ectopic bone formation was not detected when HA-TCP pellets were loaded without MSCs (Supplementary Figure 1F).

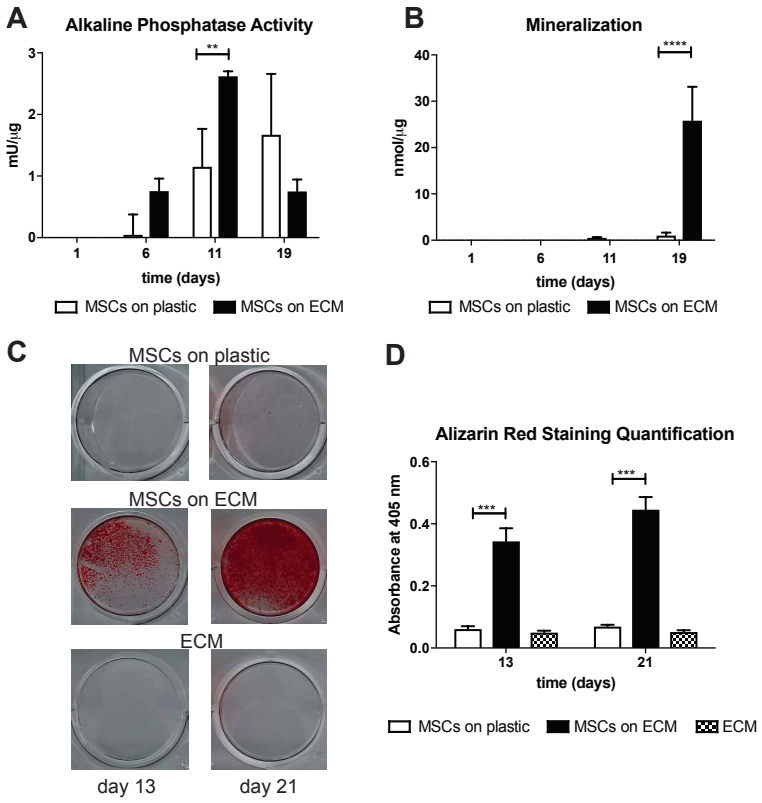

Figure 3. ECM accelerates MSC-osteogenic differentiation and mineralization. A) ALP activity in cell extracts of MSCs on ECM and plastic. B) Calcium deposition in cell extracts of MSCs cultured on ECM and plastic. The values of MSCs on ECM were subtracted by the ECM contribution. All values are corrected for protein content at each time point. Negative values were artificially set as zero. The provided results are representative of multiple independent experiments. C) Alizarin Red Staining at day 13 and 21 of culture, in MSCs on plastic (top), MSCs on ECM (middle), and ECM only (bottom). D) Quantification of Alizarin Red Staining at day 13 and 21 of culture. (**, $P<0.01$; ***, $P<0.001$, ****, $P<0.0001$). Values: Average ± SD.

The proteomic composition of the ECM corroborated the role of the devitalized matrix in mediating the observed effects on MSCs

Following these positive effects of the devitalized ECM on cell adhesion, proliferation and osteogenic differentiation of MSCs, we investigated the protein composition of the ECM, in order to identify candidate proteins and processes underlying these effects. Mass spectrometry analysis identified 846 proteins that were part of the devitalized ECM (Supplementary Table 1). Of these 846, 35 proteins were annotated as 'extracellular matrix' GO term (GO:0031012) (Figure 5A). The detection of known ECM components such as FN, COL1A1 and tenascin C (TNC) within the most abun-

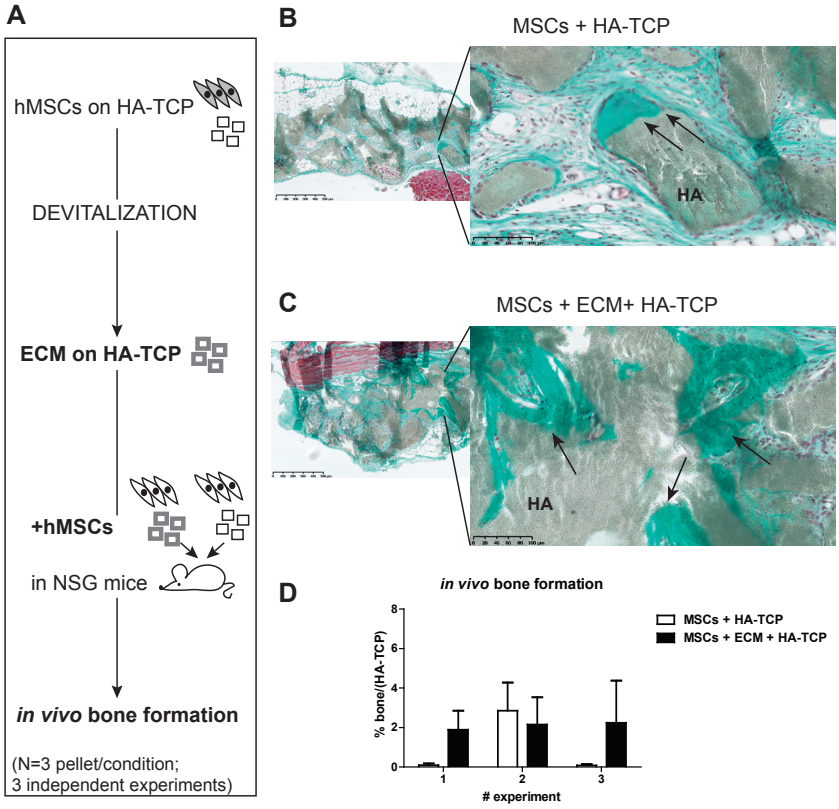

Figure 4. MSCs on ECM on HA-TCP promotes ectopic bone formation *in vivo*. A) Schematic overview of *in vivo* implantation experiment. B) Histological analysis of newly formed bone by MSCs on HA-TCP and C) MSCs on ECM on HA-TCP. Two sections/pellet, 4 pellets/conditions, in 3 independent experiment were analyzed and representative sections are shown. Arrows indicate the newly formed bone stained in green by Masson-Goldner staining on HA-TCP (indicated as HA). Light pink areas indicated unmineralized bone and purple dots indicate nuclei. Bars indicate 500 µm (left) and 100 µm (right). D) Quantification of the newly formed bone by MSCs on ECM on HA-TCP and MSCs on HA-TCP in each experiment. Three independent experiments are shown. Values: Average ± SEM of % bone/(HA-TCP) in pellets per each experiment.

dant proteins in the devitalized ECM confirmed the presence of a bone-like ECM and the validity of the devitalization treatment to produce the ECM. The presence of proteins detected by MS in the devitalized ECM such as FN, Annexin2 (ANXA2), and ALP was confirmed by Western blot analysis (Figure 5B). As illustrated in Figure 5C, GO analysis revealed that the top 10% most abundant proteins (85 proteins) were involved in cell-matrix adhesion processes, as integrin binding (GO:0005178) was significantly enriched. Furthermore, GO terms such as membrane-bounded vesicle (GO:0031988) and calcium ion binding (GO:0005509), which included proteins such as ANXA2, ANXA5 and ANXA6, were also enriched in our analysis (Supplementary

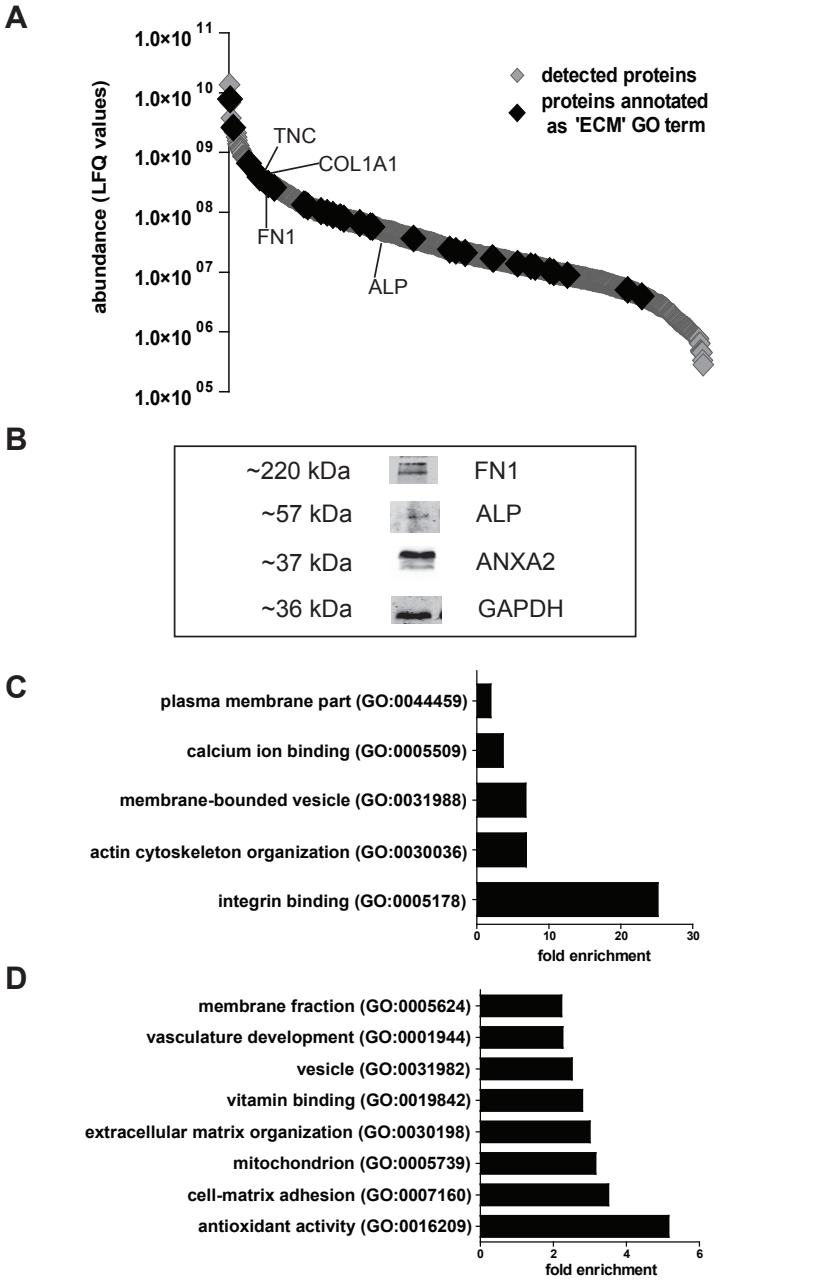

Figure 5. Proteomic analysis of the ECM composition. A) 846 proteins were detected by mass spectrometry; 35 were annotated as 'extracellular matrix' GO term. Some of the most relevant proteins are indicated. B) Western blot analysis of FN1, ALP, ANXA2 (12µg loaded) in the devitalized ECM. GAPDH was used as loading control. C) Gene ontology analysis of the top 10% most abundant detected proteins. D) Most enriched pathways of GO analysis of all the proteins detected in the ECM. Only the significantly enriched terms are shown (Benjamini P <0.01).

Table 2). As these proteins are involved in matrix-vesicle release, calcium ion binding and therefore mineralization, this suggested the role of the ECM in promoting the osteogenic differentiation and mineralization of MSCs. Alkaline phosphatase was also detected and ranked in position 142 of abundance (Figure 5A and 5B; Supplementary Table 1). However, ALP appeared to be inactive as the ECM lacked ALP activity (Supplementary Figure 1G). The GO analysis of the whole composition of the ECM shown in Figure 5D illustrates that the GO term extracellular matrix organization (GO:0030198) was significantly enriched, meaning that the total composition of ECM was important for the structure of the devitalized ECM, and not only the most abundant proteins. Furthermore, Figure 5D illustrates that GO terms such as antioxidant activity (GO:0016209), mitochondrion (GO:0005739) and vasculature development (GO:0001944) were significantly enriched (Supplementary Table 3).

The devitalized ECM showed high protein homology with human bone samples

We have previously analyzed the composition of the human bone proteome [23], showing 1213 proteins that were shared by 3 human bone samples. Further analyses lowered them down to 1200 unique proteins. This human bone proteome was compared with the protein composition of the *in vitro* cell-secreted ECM. More than 50% of the ECM proteins were shared with the bone proteome, as 473 proteins out of 846 detected in the devitalized ECM were also detected within the human bone samples (Figure 6A). Annexins such as ANXA2, ANXA6, ANXA5, ANXA1 and vimentin (VIM) were within the most abundant proteins in the ECM that were also detected in the bone proteome (Supplementary Table 4). Bioinformatic analysis of the shared proteins showed that specific osteoblast- and ECM-related terms such as 'adhesion of cell-associated ECM', 'differentiation of osteoblasts', and 'proliferation of connective tissue cells', were significantly enriched (Figure 6B), confirming the role of the protein composition of the ECM in mediating these effects. Proteins such as trombospondin-1 (THBS1), VTN and FN, but also intracellular proteins such as integrins, were within the 473 shared proteins, and were involved in 'adhesion of cell-associated matrix'. Moreover, proteins such as SPARC, COL1A1 and fibulin-1 (FBLN1) were related to the proliferation of connective tissue cells, whereas TNC, VIM and Versican (VCAN) were responsible for the differentiation of osteoblasts, overall confirming the role of the ECM in mediating the functional effects we observed.

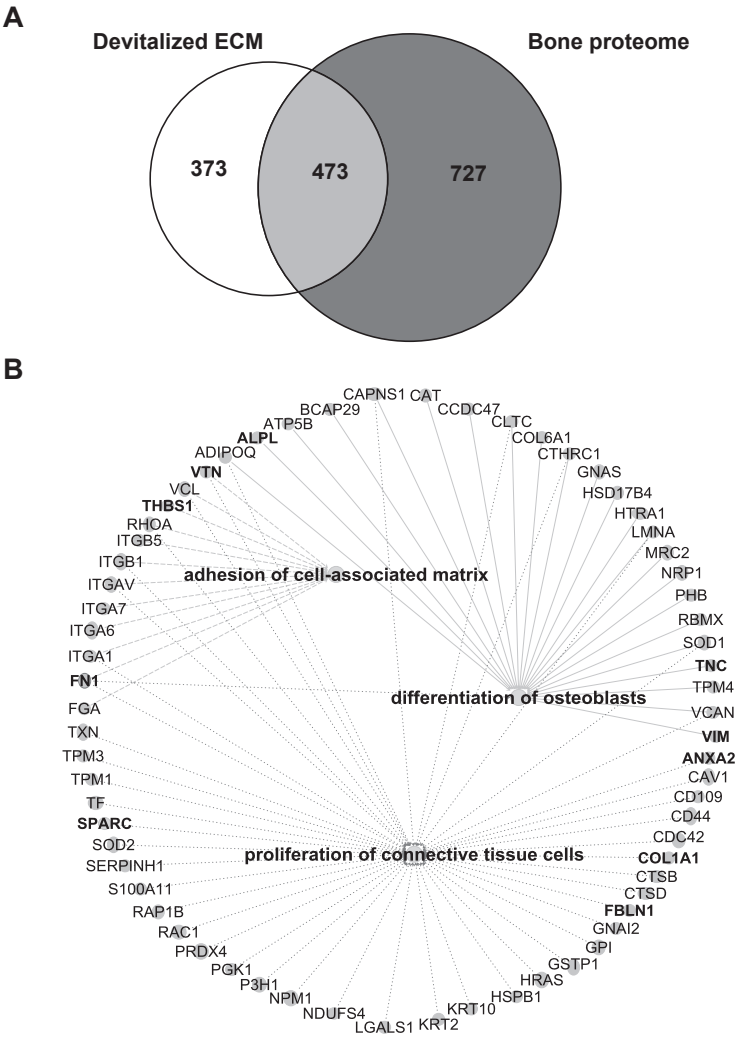

Figure 6. Comparison of the protein composition of the devitalized ECM and the human bone proteome. A) 473 proteins were shared between the devitalized ECM and the human bone proteome. B) Ingenuity Pathway Analysis of the 473 proteins shared between the devitalized ECM and the human bone samples. Represented proteins lead to the significant enrichment of Functional Annotations such as 'proliferation of connective tissue cells' (P=3.81 E-09), 'differentiation of osteoblasts' (P=6.44 E-07) and 'adhesion to cell-associated matrix' (P=1.89 E-06) (bold: proteins highlighted in the text).

DISCUSSION

In this study, we successfully produced an osteopromotive human MSC-derived ECM, which was able to accelerate the adhesion, proliferation and osteogenic potential of MSCs *in vitro* and to promote ectopic bone formation *in vivo*. Known ECM

components were detected in the devitalized ECM, which also showed high homology with the human bone protein composition. This validated our ECM-model and provided insights into how the ECM may modulate MSC-behavior. Moreover, many unexpected proteins not directly related to ECM-structural role were also detected.

Immediately after seeding on the ECM, MSCs formed focal-adhesion-complexes that improved their adhesion to the devitalized ECM. Extracellular proteins, such as FN, COL1A1, VTN and TNC, favor osteoblast adhesion to the ECM by creating cell-matrix adhesion sites [6, 20]. The proteomic analysis of the devitalized ECM identified FN, COL1A1 and TNC within the most abundant proteins, and other adhesive extracellular proteins, such as VTN and FBLN1. Together this confirmed the presence of cell-adhesion promotors in the devitalized ECM, explaining the accelerated cell attachment. Moreover, the devitalized ECM was able to enhance the attachment of MSCs irrespectively of their commitment, as less committed cells attached on the ECM to a similar extent than the more committed ones.

One day on the devitalized ECM was already sufficient to increase the percentage of proliferating MSCs, confirming previous findings that used different cell-secreted ECMs to enhance MSC proliferation [11-13, 16]. By analyzing the proteomic composition of the ECM, we could successfully detect FN, COL1A1 and SPARC, which have been shown to promote osteoblast proliferation [22, 32], and TNC, which may mediate transforming growth factor beta (TGF-β) action on bone formation [33]. The percentage of proliferating cells decreased over time as cells started to differentiate.

The devitalized ECM induces a faster differentiation of MSCs toward mineralizing osteoblasts as both ALP activity and matrix mineralization were higher when MSCs were cultured on the ECM. This observation is supported by previous findings showing *in vitro* cell-secreted-ECMs that promoted osteogenesis [14, 15]. The quicker adhesion to the known osteogenic inducers that were detected in the ECM, such as COL1A1, FN, collagen type XII alpha 1 (COL12A1), TNC, VTN and SPARC, might activate integrin-mediated signaling pathways, increasing osteogenic differentiation [5, 20, 22, 33, 34]. Annexins such as ANXA2, ANXA5 and ANXA6 were detected in the devitalized matrix, along with previous findings [17]. Annexins are the initiators of mineralization and were also detected within the most abundant proteins in human bone samples, confirming the role of the devitalized ECM in mimicking the osteogenic bone microenvironment [23, 35]. Despite the detection of initiators of mineralization such as Annexins and ALP, the ECM has low ALP activity and does not mineralize without the further presence of living cells. The necessity of living cells may be conceptually important for the therapeutic application of devitalized ECM. If the ECM mineralizes independently of living cells, this would lead to uncontrolled mineralization, and may lead to pathological heterotopic mineralization. As osteoblast differentiation and bone formation are complex processes in which timing,

order and magnitude of events are important, inappropriate timing of mineralization thus may lead to an inappropriate bone repair process.

Bone formation induced by ECM directly implanted *in vivo* or by MSCs expanded on ECM *ex-vivo*, have shown conflicting findings [10]. We showed that the ECM promoted *in vivo* ectopic bone formation by MSCs, inducing a higher amount of bone than by MSCs alone. Probably the role of ECM is decisive to stimulate a robust formation of bone. However, further experiments are needed to increase the sample size and diminish the heterogeneity to overcome the biological variation. Based on our current observations we propose that with any given MSC preparation, one may or may not observe bone formation, whereas in the presence of the ECM we produced, bone formation will be observed with all MSC preparations. In other words, the presence of the ECM seemed to reduce variation in the amount of bone formed over different experiments.

Structural ECM proteins and known components of the bone marrow niche, such as COL1A1, FN, VTN and TNC, were successfully detected among the most abundant proteins in the ECM, along with previous findings [12, 16-18]. However, also inhibitors of mineralization were detected, such as alpha-2-HS-glycoprotein (AHSG), which is found in the mineralized bone but also acts as inhibitor of ectopic calcification [36]. Interestingly, growth factors such as BMPs and TGF-β could not be detected in the ECM, which may be attributed to the sensitivity of the technique or to the devitalization procedure. Despite the absence of GFs, we unequivocally show that the matrix influenced MSC behavior. Probably, ECM-remodeling takes place, releasing GFs that were entrapped in the ECM. Indeed, protease inhibitors such as cystatin C (CST3), were detected, but also proteinases, such as matrix metalloproteinase 14 (MMP14), which are known to promote osteogenic differentiation [37, 38].

Notably, many proteins detected in the devitalized matrix were annotated as cytoplasmic or plasma membrane-bound. Cell-remnants most likely arose from cell-lysis during the freeze-thaw cycling and were resistant to the extensive washings [10]. Nevertheless, we should consider that the ECM-composition in its entirety was responsible for the effects described in this study; these proteins enriched the matrix composition, playing a central role with the known ECM proteins. As more than 50% proteins were shared between the devitalized ECM and the human bone samples, we thus show that our natural ECM model is representative of the *in vivo* dynamic bone microenvironment. Following this, cell-remnants may have a functional role as remnants arising from osteoblasts undergoing apoptosis. These are present in the bone and bone-marrow and stimulates efferocytosis by osteal macrophages, which are key regulators of bone homeostasis and wound repair [39]. Therefore, the cell-remnants detected in the devitalized ECM could implement the supportive role of stromal cells and thereby the ECM we produced may represent a more complete

environment than just the well-known ECM proteins. However, further studies are needed to unravel new functions for the ECM in the context of osteoimmunology.

We unexpectedly detected many proteins related to mitochondrial functions and structure in the devitalized matrix. Nevertheless, we show that the devitalized matrix is metabolically inactive. As the osteogenic differentiation is a high-energy demanding process, we believe that these proteins arise from lysis of the ECM-secreting MSCs, as the devitalization occurred before the onset of mineralization and might be related to energy metabolism function.

Gene ontology analysis of the proteins detected in the ECM revealed also GO terms that were not directly related to known ECM-functions, thus broadening the spectrum of the devitalized ECM functions. For instance, 'Antioxidant activity' appeared as an enriched GO term, with proteins such as superoxide dismutase 1 (SOD1) that was previously detected in the human bone microenvironment [23]. As the ECM has been already proposed to reduce MSC aging [13], the antioxidant function of the devitalized matrix should be further investigated to improve *ex-vivo* cultures for clinical applications. The most abundant proteins detected in the matrix were also related to angiogenesis and vasculature remodeling, showing interesting functions of the ECM. Indeed, among these proteins, TNC is mitogenic for hematopoietic stem cells (HSCs) in HSC-niche, [40] and COL1A1 is involved in vasculature remodeling [41]. Our findings support the idea of using the matrix for HSC expansion [16].

The role of ECM in modulating MSC-behavior has been successfully investigated in many studies using cell-secreted ECMs, that have been obtained by different decellularization techniques. Although the freeze/thaw cycles approach has been shown to damage the fibrillary structure of ECM [42], and not removing all cell-remnants, this method also allowed successful production of cell-derived ECMs on scaffolds and maintain most of the ECM components [10, 14, 43]. Along with these latter findings, we believe that the model of devitalized ECM presented here represents a simpler way to produce a matrix *in vitro* by using cost-effective freeze/thaw cycling, while still being able to accelerate and improve the osteogenic potential of MSCs as shown. In summary, we produced an osteoblast-derived ECM by a simple devitalization treatment; this *in vitro* model of bone-ECM improved the osteogenic potential of MSCs, reinforcing previous findings. This, combined with the increase in cell proliferation could be useful to expand autologous MSCs *ex-vivo* and improve their use for bone regeneration. A detailed proteomic analysis revealed known ECM components responsible for the observed effects and an overlap with the human bone microenvironment, but also novel ECM functions that need further investigation. Some candidate proteins could be overexpressed in ECM-secreting MSCs, to produce a tailor-made ECM that improves MSC properties to accelerate fracture healing, broadening the future applications of the cell-secreted ECM. In ad-

dition, MSCs could be isolated from patients to easily produce an autologous ECM, to improve patient-specific therapies. Overall, the devitalized ECM could be applied as natural biomaterial that mimics the osteogenic niche and to functionalize scaffolds to develop osteoinductive materials for the implanted cells *in vivo,* in order to robustly accelerate bone regeneration.

ACKNOWLEDGEMENTS

Funding: This work was supported by a grant from the Dutch government to the Netherlands Institute for Regenerative Medicine (NIRM, grant No: FES0908) and Erasmus Medical Center. The authors thank Molecular Medicine Post Graduated School, T. Strini and C. S. van der Leije for technical assistance, P. Kumar for performing Western blots, Dr. L. Sasso, Dr. H. H Perez Garza and Dr. M. K. Ghatkesar for helping with atomic force microscopy and data interpretation, and K. Bezstarosti and D. Dekkers for mass spectrometry analysis.

Author Contributions: MB, BE, RA, JP, JL designed research. MB, SC, ERT, IE, YK, MK performed research. MB, BE, SC, ERT, IE, LFA, YK, MK, JD, JP, JL analyzed data. MB; JP, JL drafted manuscript. MB, BE, JP, RA, JL revised the final version of manuscript. All authors have approved the final article.

No competing financial interest exists.

REFERENCES

1. Caplan, A.I., *Mesenchymal stem cells.* J Orthop Res, 1991. 9(5): p. 641-50.
2. Pittenger, M.F., et al., *Multilineage potential of adult human mesenchymal stem cells.* Science, 1999. 284(5411): p. 143-147.
3. Caplan, A.I., *Review: mesenchymal stem cells: cell-based reconstructive therapy in orthopedics.* Tissue Eng, 2005. 11(7-8): p. 1198-211.
4. Sommerfeldt, D.W. and C.T. Rubin, *Biology of bone and how it orchestrates the form and function of the skeleton.* Eur Spine J, 2001. 10 Suppl 2: p. S86-95.
5. Alford, A.I., K.M. Kozloff, and K.D. Hankenson, *Extracellular matrix networks in bone remodeling.* Int J Biochem Cell Biol, 2015. 65: p. 20-31.
6. Hidalgo-Bastida, L.A. and S.H. Cartmell, *Mesenchymal stem cells, osteoblasts and extracellular matrix proteins: enhancing cell adhesion and differentiation for bone tissue engineering.* Tissue Eng Part B Rev, 2010. 16(4): p. 405-12.
7. Hynes, R.O., *The extracellular matrix: not just pretty fibrils.* Science, 2009. 326(5957): p. 1216-9.
8. Guilak, F., et al., *Control of stem cell fate by physical interactions with the extracellular matrix.* Cell Stem Cell, 2009. 5(1): p. 17-26.
9. Badylak, S.F., D.O. Freytes, and T.W. Gilbert, *Extracellular matrix as a biological scaffold material: Structure and function.* Acta Biomater, 2009. 5(1): p. 1-13.
10. Fitzpatrick, L.E. and T.C. McDevitt, *Cell-derived matrices for tissue engineering and regenerative medicine applications.* Biomater Sci, 2015. 3(1): p. 12-24.
11. Chen, X.D., et al., *Extracellular matrix made by bone marrow cells facilitates expansion of marrow-derived mesenchymal progenitor cells and prevents their differentiation into osteoblasts.* J Bone Miner Res, 2007. 22(12): p. 1943-56.
12. Lai, Y., et al., *Reconstitution of marrow-derived extracellular matrix ex vivo: a robust culture system for expanding large-scale highly functional human mesenchymal stem cells.* Stem Cells Dev, 2010. 19(7): p. 1095-107.
13. Sun, Y., et al., *Rescuing replication and osteogenesis of aged mesenchymal stem cells by exposure to a young extracellular matrix.* FASEB J, 2011. 25(5): p. 1474-85.
14. Datta, N., et al., *Effect of bone extracellular matrix synthesized in vitro on the osteoblastic differentiation of marrow stromal cells.* Biomaterials, 2005. 26(9): p. 971-7.
15. Mauney, J.R., D.L. Kaplan, and V. Volloch, *Matrix-mediated retention of osteogenic differentiation potential by human adult bone marrow stromal cells during ex vivo expansion.* Biomaterials, 2004. 25(16): p. 3233-43.
16. Prewitz, M.C., et al., *Tightly anchored tissue-mimetic matrices as instructive stem cell microenvironments.* Nat Methods, 2013. 10(8): p. 788-94.
17. Kolf, C.M., et al., *Nascent osteoblast matrix inhibits osteogenesis of human mesenchymal stem cells in vitro.* Stem Cell Res Ther, 2015. 6: p. 258.
18. Marinkovic, M., et al., *One size does not fit all: developing a cell-specific niche for in vitro study of cell behavior.* Matrix Biol, 2016. 52-54: p. 426-41.
19. Ragelle, H., et al., *Comprehensive proteomic characterization of stem cell-derived extracellular matrices.* Biomaterials, 2017. 128: p. 147-159.
20. Salasznyk, R.M., et al., *Adhesion to Vitronectin and Collagen I Promotes Osteogenic Differentiation of Human Mesenchymal Stem Cells.* J Biomed Biotechnol, 2004. 2004(1): p. 24-34.

21. Santiago, J.A., R. Pogemiller, and B.M. Ogle, *Heterogeneous differentiation of human mesenchymal stem cells in response to extended culture in extracellular matrices.* Tissue Eng Part A, 2009. 15(12): p. 3911-22.
22. Ode, A., et al., *Toward biomimetic materials in bone regeneration: functional behavior of mesenchymal stem cells on a broad spectrum of extracellular matrix components.* J Biomed Mater Res A, 2010. 95(4): p. 1114-24.
23. Alves, R.D., et al., *Unraveling the human bone microenvironment beyond the classical extracellular matrix proteins: a human bone protein library.* J Proteome Res, 2011. 10(10): p. 4725-33.
24. van Hengel, I.A.J., et al., *Selective laser melting porous metallic implants with immobilized silver nanoparticles kill and prevent biofilm formation by methicillin-resistant Staphylococcus aureus.* Biomaterials, 2017. 140: p. 1-15.
25. Horzum, U., B. Ozdil, and D. Pesen-Okvur, *Step-by-step quantitative analysis of focal adhesions.* MethodsX, 2014. 1: p. 56-9.
26. Bruedigam, C., et al., *Basic techniques in human mesenchymal stem cell cultures: differentiation into osteogenic and adipogenic lineages, genetic perturbations, and phenotypic analyses.* Curr Protoc Stem Cell Biol, 2011. Chapter 1: p. Unit1H 3.
27. Abdallah, B.M., N. Ditzel, and M. Kassem, *Assessment of bone formation capacity using in vivo transplantation assays: procedure and tissue analysis.* Methods Mol Biol, 2008. 455: p. 89-100.
28. Morhayim, J., et al., *Proteomic signatures of extracellular vesicles secreted by nonmineralizing and mineralizing human osteoblasts and stimulation of tumor cell growth.* FASEB J, 2015. 29(1): p. 274-85.
29. Vizcaino, J.A., et al., *2016 update of the PRIDE database and its related tools.* Nucleic Acids Res, 2016. 44(22): p. 11033.
30. Huang da, W., B.T. Sherman, and R.A. Lempicki, *Systematic and integrative analysis of large gene lists using DAVID bioinformatics resources.* Nat Protoc, 2009. 4(1): p. 44-57.
31. Alves, R.D., et al., *Activin A suppresses osteoblast mineralization capacity by altering extracellular matrix (ECM) composition and impairing matrix vesicle (MV) production.* Mol Cell Proteomics, 2013. 12(10): p. 2890-900.
32. Globus, R.K., et al., *Fibronectin is a survival factor for differentiated osteoblasts.* J Cell Sci, 1998. 111 (Pt 10): p. 1385-93.
33. Mackie, E.J., et al., *Regulation of tenascin-C expression in bone cells by transforming growth factor-beta.* Bone, 1998. 22(4): p. 301-7.
34. Delany, A.M., et al., *Osteonectin-null mutation compromises osteoblast formation, maturation, and survival.* Endocrinology, 2003. 144(6): p. 2588-96.
35. Anderson, H.C., R. Garimella, and S.E. Tague, *The role of matrix vesicles in growth plate development and biomineralization.* Front Biosci, 2005. 10: p. 822-37.
36. Schafer, C., et al., *The serum protein alpha 2-Heremans-Schmid glycoprotein/fetuin-A is a systemically acting inhibitor of ectopic calcification.* J Clin Invest, 2003. 112(3): p. 357-66.
37. Karsdal, M.A., et al., *Matrix metalloproteinase-dependent activation of latent transforming growth factor-beta controls the conversion of osteoblasts into osteocytes by blocking osteoblast apoptosis.* J Biol Chem, 2002. 277(46): p. 44061-7.
38. Danjo, A., et al., *Cystatin C stimulates the differentiation of mouse osteoblastic cells and bone formation.* Biochem Biophys Res Commun, 2007. 360(1): p. 199-204.
39. Sinder, B.P., A.R. Pettit, and L.K. McCauley, *Macrophages: Their Emerging Roles in Bone.* J Bone Miner Res, 2015. 30(12): p. 2140-9.

40. Klein, G., S. Beck, and C.A. Muller, *Tenascin is a cytoadhesive extracellular matrix component of the human hematopoietic microenvironment.* J Cell Biol, 1993. 123(4): p. 1027-35.
41. Wang, Z. and N.C. Chesler, *Role of collagen content and cross-linking in large pulmonary arterial stiffening after chronic hypoxia.* Biomech Model Mechanobiol, 2012. 11(1-2): p. 279-89.
42. Tour, G., M. Wendel, and I. Tcacencu, *Cell-derived matrix enhances osteogenic properties of hydroxyapatite.* Tissue Eng Part A, 2011. 17(1-2): p. 127-37.
43. Thibault, R.A., et al., *Osteogenic differentiation of mesenchymal stem cells on pregenerated extracellular matrix scaffolds in the absence of osteogenic cell culture supplements.* Tissue Eng Part A, 2010. 16(2): p. 431-40.

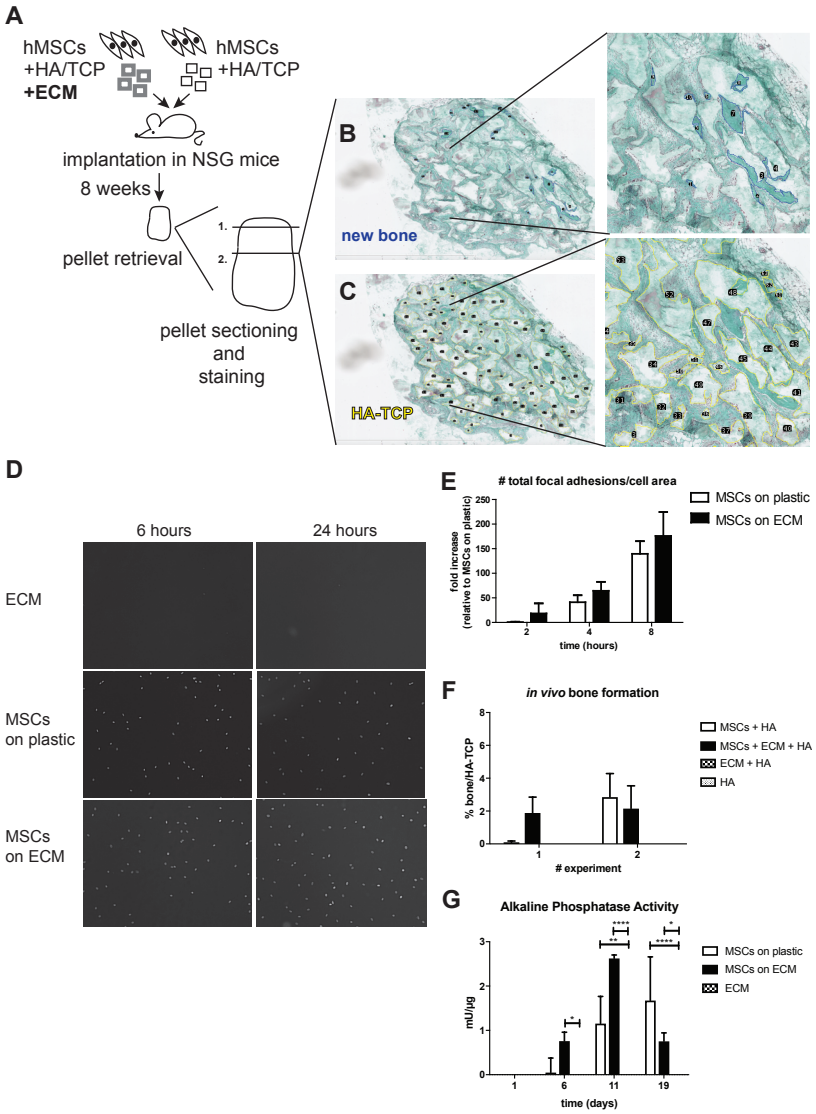

Supplementary Figure 1. A) Schematic representation of *in vivo* ectopic bone formation analysis. MSCs on HA-TCP with and without ECM were implanted in NSG mice and pellets were retrieved 8 weeks after implantation. Two sections/pellet were stained with Goldner staining. To determine the percentage of newly formed bone, area of Goldner staining-positive newly formed bone (B) (indicated as 'new bone' in blue) over HA-TCP areas (C) (indicated as HA-TCP in yellow) were quantified. D) DAPI staining of devitalized ECM and of MSCs cultured on ECM and on plastic for 6 and 24 hours. E) Quantification of cell adhesion at 2, 4, 8 hours after seeding (number of focal adhesions/cell area). F) Quantification of the newly formed bone by MSCs on ECM on HA-TCP, MSCs on HA-TCP and by ECM on HA-TCP and HA-TCP as control in each experiment. Two independent experiments are shown. Values: Average ± SEM of % bone/(HA-TCP) in pellets per each experiment. G) ALP activity measured in lysates from ECM and MSCs cultured on plastic and ECM for 19 days (*, $P<0.05$, **, $P<0.01$; ****, $P<0.0001$). Negative values were artificially set as zero. Values: Average ± SD.

Supplementary Table 1. List of proteins detected in the devitalized ECM. Proteins are indicated as protein IDs and ranked for abundance. The top 10% (85) most abundant proteins are indicated in bold.

P63261	**P07099**	P09525	Q53GQ0	P09622	P08238
P07355	**CON__Q0IIK2**	P49257	O94925-3	O75947	C9J3L8
CON__P02769	**E9PNW4**	P04899	P47985	F8VNT9	I3L1P8
P04264	**Q9UHG3**	Q04941	Q5JPE7-2	Q9UKX5	P46977
P15144	**Q14764**	Q15084-3	O95202	R4GN98	P14384
P08133	**P04792**	P22695	O95831-3	P31040	Q13724-2
P08758	**P40939**	P24539	P50995-2	Q99623	Q9NRP0
CON__P12763	**Q01995**	F5GXX5	P62937	P60981	B4DZI8
P13645	**Q00325-2**	P18206-2	P19105	E9PR44	Q04837
P06576	**P49755**	P08195-2	P35232	P30084	O60831
Q14195	**P23284**	P09619	P11498	P07954-2	P61604
P35908	**P40926**	P09493-3	Q99715-4	Q96IX5	P30040
REV__S4R403	**P04406**	P35613-2	Q9BWM7	Q01628	Q5JP53
P14625	**P38646**	P31949	P17813-2	O00483	Q9Y2Q3
P11021	**P00367**	P48047	P28331-4	Q10472	P08574
P35527	**E9PIM6**	P20340-2	P51659	Q13162	K7EJE8
Q13740-2	**P24821-4**	P11279	P51148	Q92743	Q969X5-2
P00387-2	**P02452**	P49748-2	Q99798	P13611-2	P61009
P04083	**P12236**	P60903	O15173	P36957	P05141
P35579	**P43121**	P13073	P30050	E7ETY7	Q9UJS0
P25705	**Q9BVK6**	Q96AG4	J3QS39	Q9H9B4	P05388
P68032	**P39656**	P31930	P54709	Q9BSJ8	Q9NYL4-2
CON__P34955	**Q9Y6N5**	Q70UQ0-4	CON__EN-SEMBL:ENS-BTAP00000016046	P56385	P24752
P27824	**P02545-2**	P07339		P26038	CON__Q2KIS7
P04843	**CON__Q3SX09**	P21589		Q3SY69	P21912
P21333-2	**Q13423**	P09382	Q15758	P60174-1	CON__Q9TRI1
P08670	**P51571**	Q15363	P10620	P24390	Q8WWI5-3
Q09666	**P02751-17**	P00403	P22307-6	Q86UY0	P30044-2
G5EA52	**O43707**	H0YD13	P62805	B1AH87	O75489
P12814	**P36269**	Q8IWA5-3	Q15836	B7Z6B8	O15460-2
P05556	**Q14108**	Q5VTE0	C9JA28	P62258	Q12797-10
CON__P15497	**Q07065**	P60468	Q02218	P26006	P08779
Q6UVK1	Q6DD88	P12111-2	P56134-3	P52907	P61619
Q9NZM1-6	P06733	P05186	Q6YHK3	CON__P17690	REV__H0Y547
P10809	P23634-7	P45880	P63104	B4E2S7	P04075
P27797	P21964-2	E9PN17	P04179-4	P11047	B4DT77
P50454	P61224	Q9BVC6	Q99880	Q96JJ7	Q9BS26
P04844	P18084	Q9Y4L1	P27658	P13674	Q00765
P08648	Q2Y0W8-5	P00338	Q99878	Q9UGT4	Q14165
E9PJK1	O75396	REV__Q96HY7	P10301	P07996	O15427
P56199	Q9HDC9	Q12907	Q9P0L0	Q32P28	P04062-4
P21796	P30048-2	J3KNF8	P55084-2	P84077	P67936
Q03135	Q9UBI6	P61106	Q71U36-2	P42704	Q9Y5U9
P05023-4	P16615-5	P14314-2	P08123	O95302	P30049
P06756-3	P11142	P55072	B4E2V5	Q15149	CON__Q3SZ57
P06396-2	P61019	Q6NZI2	Q15165-3	Q00610-2	P62820
P07237	F8W1R7	P04040	P00167-2	Q05682-5	Q8TCT9-5
Q14697	P23528	P30447	H0YNG3	P29992	P12109
Q9NQC3-2	Q9H0U4	P51572	B4DJV2	P07737	P07942
Q9UBG0	P14618	P61026	Q969H8	Q15005	Q16563-2
CON__EN-SEMBL:ENSBTAP00000024146	CON__P01966	Q9BTV4	Q12884	P07951-2	J3KTF8
	O75915	Q96AY3	P13667	Q6NUK1	P13647
	P62873	Q9NYU2-2	Q9Y3B3-2	E9PMR4	Q9P2E9
Q07954	P51149	B4DMK0	Q9NVJ2	P02786	P11177-2
Q08431	Q9Y490	O15260-2	Q99714	I3L4X2	P02538

O43852
P54289-4
CON__Q3ZBS7
Q99536
P60059
Q8N766-3
A6NNI4
P61981
P39019
Q92520
CON__Q58D62
O95197-3
Q7Z3B1
Q06830
P49419-2
Q9H3N1
P54920
Q01082
P14406
Q7Z7H5-3
G3XAM7
P05091
E9PEP6
Q92896
P63000
P61586
P31946-2
Q9Y639-1
P00505
F8VQX6
P22392-2
O95980
Q13011
P53007
O60762
P34897-3
Q9HC07
P50213
B4DL14
O94919
Q9Y3A6
CON__Q3MHN5
P43304-2
Q9BQB6-3
P50416-2
P46783
P11233
Q9Y5M8
P14209
P59998
P02533
O00116
O15031
P16435
Q9Y394-2
P30519
Q07021
P41250
P60953
Q99805
Q969V3-2
P09669
Q96I99
P26885
P46940
P61769
O14735-3
P35052
Q99720
Q8N0U8
Q9UIJ7
P11717
Q96HE7
O14495
K7EMV3
Q8NB49-2
P21397
Q5ZPR3-3
P09486
P50148
P51636-2
Q8TCJ2
Q9UFN0
P55290
P48357-5
O00469
J3QS48
Q9UBV2
P62913-2
B4DEZ3
Q02809
CON__Q2KJF1
P09211
Q9Y3E5
O75487
P38117
O75844
Q5JRX3
Q96G23
P62269
Q96D15
Q9UIQ6-3
P22314
O94875-9
P47756-2
J3KN67
Q9Y6A9
P62879
P42126-2
Q13813-3
P62736
Q9UL25
O14880
Q9UHA4-2
O75531
P55809
J3QQY2
P09110
A6NLH6
Q8N6L1
Q9P035
P01112
P40261
Q969G5
E5RI99
Q14699
CON__P01044-1
A8MWK3
O14949
E7ENA9
H0YFI1
E7EMM4
P14854
Q5RI15
Q53TN4-3
P06744
Q04917
CON__ENSEMBL:ENS-
BTAP00000007350
H0YL12
O75891
K7ERI7
CON__Q9TTE1
P49914-2
Q9HCU0
Q9UDW1
O60568
P05387
Q6PIU2
E7ESK6
Q9UJZ1-2
P63092-3
Q86UE4
P18669
Q86WV6
O95292
O75369-2
E9PN66
Q4G0P3
Q99523
Q9Y4D7-2
F8W031
P07858
P42765
M0QZN2
P0CW22
P11234
P19404
Q9Y2R0
P12235
P10606
P14927
P04632
X6RJP6
F8W7Q4
P61421
Q5T092
P27348
F5H8J3
Q8TBQ9
G3V1S6
P55145
Q96A33-2
O94826
Q9NS69
O00264
P13639
P05362
O95168-2
P12110-3
Q9HD45
Q6ZUX7
P04181
Q16740
P61158
P53621
H3BN98
P84157-2
P07900
P17342-2
O15144
P23396
O15254-2
P00558
CON__Q3SZV7
P54886-2
E9PH64
P61326
Q5BJH7-6
Q8N5M9
Q86Y82
O15400-2
Q14118
P57088
Q9NZN4
Q9Y3D7
Q08722-2
Q5R3B4
Q8N4V1
F5H6U7
Q9Y6C2
Q7Z4H8
Q8N1B9
P62081
O95479
P30483
P43007
P07602
F6WST4
P16278-3
E9PNJ4
Q14240
G3V5P8
F6SBX2
Q9Y2Q5
Q9UI09
P62750
B4DJA5
Q8N5K1
O96000
Q9HAV0
E9PP23
P48449-2
Q86YZ3
Q9BXK5-4
P08107
P00441
P30038
Q8NBX0
P10321
Q9NP72
Q16555
P31937
P16112-2
Q01518-2
O14828-2
Q9Y680-3
P36871
C9JEN3
P47755
P24844
Q5JTV8
P18085
O75083
C9JFR7
P08559-3
O15118
O95298
P10599
M0QZY4
P11166
Q96S97
Q9NTJ5
Q9Y277
Q8N2H3
E7EQU2
G3V1B6
Q9NZ45
C9JP16
Q06136
H0YJ40
Q01650
Q9P0S9
Q02252-2
P62906
Q8IVL6-2
P05109
Q16134-3
O15121
Q3ZCQ8

P62851
P48960-2
P61160
O14494
P20020-5
Q08257-3
M0R3D4
Q7KZF4
E5RHW4
O14548
P57105
O75306-2
O95183
O43399-2
Q86UP2-2
O15511
H7BZ81
Q9H251-5
Q9BU23-2
P51970
Q86UY8
Q9H061
Q16836
P32969
P03928
O75746
Q99470
Q9Y673-2
B4DGU4
P55769
O43920
O43678
Q9H3Z4-2
Q96DZ1-3
Q0ZGT2-4
Q9H4G4
Q9HB66
Q86Y39
Q9NR31
Q9BRR6-2
P38919
P26022
Q12931-2
P30837
P61006
P23368
Q8WY22
Q9NZ01
P41159
Q15006
Q6ZXV5-2
J3QRD1
Q6YN16
G3XAN4
C9JKQ2
Q9C0E8-2
Q9BQE5
P62834
F8WBE2
CON__Q03247
Q8NBJ7
B4DKB2
E7EPM6
O15439-2
H3BSC1
Q14254
P60866
Q15293
CON__Q3Y5Z3
Q13683-9
P53597
E5RIP4
Q6UXV4
E9PIE4
Q7Z5G4
REV__Q5JVD3
O15269
H3BR27
Q13636
O60613
Q9H0R3-2
Q9H2U2-6
Q13641
Q4KMQ2-3
Q92544
J3QRU4
O95169-3
E5RK01
Q9UP95-3
Q9UBS4
P49821-2
Q9BUB7-2
Q99643-5
O14579
Q9H330-2
P50281
Q5T123
Q9NX40
F5H0J3
Q9Y696
O75955
CON__P07224
P28066
P10619-2
K7ENI6
Q15404-2
REV__Q86VH2-3
H7BXI1
O00161-2
Q14696
P61020
Q9HAV7
CON__Q3T052
P02656
E9PN51
P50395
P27701-2
Q6P587
O60701
B4DLH2
Q96CG8-3
Q8NE86-3
Q15738
H7C2G3
P23229-4
Q92629-3
Q9HD20-2
J3QL56
Q6PI78
O43504
Q13505-3
Q15155
Q8NBJ5
H0YDT8
P63173
Q96CS3
O43181
Q92633
CON__P02777
REV__CON__P02672
Q9BWH2
P51809-3
REV__M0R0Q7
Q5XKP0
O95573
Q6IAK0
F8WAS3
O14656
P03897
O96011-2
O95571
Q9Y5J7
Q9Y305-3
H7BZI1
Q9H1E5
Q7Z7M9
P81605
Q5JX45
Q9Y584
REV__H7C388
Q9H0U3
C9JGJ9
P84095
B4DQ51
B4DN67
E9PCB6
Q9BW60
C9JL85
Q9H3H5-3
D6RBS5
Q969M3
S4R3U9
P02461-2
F8VQW8
H0Y8Z9
S4R329
G3V5T4
A8MT40
Q14739
Q5T7F5
P01034
P23786
Q9Y320-2
Q9BRK3-3
Q9HBH5
O14521-2
P28838-2
F5H261
H0YLB6
O15438
Q96QK1
H0YHJ8
Q9UM54-5
P06748-2
REV__Q5T4B2-2
F5H5N1
Q9UGQ3-2
Q6UWP7-3
P08842
Q8WVX3
Q9P0J1
F8WAX7
I3L1T3
Q8NFQ8
H0YC95
Q6TDP4
E9PP42
C0H5Y7
O94911
U3KQU4
F5H459
B5MCE2
P08473
C9JY28
K7EP56
P52815
Q9NZ08
H7BXK9
M0R1E0
P00156
H7C613
Q5T3Q7
H7BXL1
F5H4N4
E9PSI1
D6RF69
O75051
P05771
H7BYE5
H0YNE5
Q7KYR7-6

Supplementary Table 2. List of proteins belonging to the indicated GO terms (Benjamini *P*<0.01) of the GO analysis of the top 10% most abundant proteins in the devitalized ECM. Proteins are indicated as Gene names.

Category	GO term		Count	Genes	Fold Enrichment	Benjamini *P* value
GOTERM_MF_FAT	GO:0005178	integrin binding	8	ACTN4, ITGA5, ITGA1, ACTN1, MFGE8, CALR, ITGB1, THY1	25.15	7.16E-06
GOTERM_BP_FAT	GO:0030036	actin cytoskeleton organization	9	ACTG1, ACTC1, ACTN4, GSN, ACTN1, MYH9, CALR, ITGB1, FLNA	6.82	0.008471569
GOTERM_CC_FAT	GO:0031988	membrane-bounded vesicle	24	P4HB, TF, A2M, GANAB, PDIA3, ACTN4, ITGA1, ACTN1, ANPEP, ATP1A1, ITGB1, CANX, ANXA2, ANXA6, HSP90B1, APOA1, LRP1, PPIB, ALB, RPN1, TMED10, HSPA5, HSPD1, FN1	6.75	1.75E-11
GOTERM_MF_FAT	GO:0005509	calcium ion binding	18	ACTN4, ATP5B, MRC2, ITGA1, ANXA1, ACTN1, ANXA5, CALR, CANX, ANXA2, ANXA6, HSP90B1, LRP1, ITGA5, GSN, ITGAV, HSPA5, SSR4	3.63	4.30E-04
GOTERM_CC_FAT	GO:0044459	plasma membrane part	26	CYB5R3, TF, CAV1, CSPG4, ANPEP, CALR, ITGB1, ALCAM, ANXA6, ITGAV, SLC25A3, SCARB2, SSX2IP, FN1, ANXA1, ITGA1, ACTN1, MFGE8, ATP1A1, MYH9, THY1, LRP1, ITGA5, CD59, CD81, HSPD1	1.89	0.007441549

Supplementary Table 3. List of proteins belonging to the indicated GO terms (Benjamini *P*<0.01) of the GO analysis of all proteins in the devitalized ECM. Proteins are indicated as Gene names.

Category	GO term		Count	Genes	Fold Enrich-ment	Benjamini *P* value
GOTERM_MF_FAT	GO:0016209	antioxidant activity	12	MGST3, ALB, APOE, GSTK1, PRDX4, PRDX5, GPX8, PRDX3, CAT, SOD1, PRDX1, SOD2	5.16	3.57E-04
GOTERM_BP_FAT	GO:0007160	cell-matrix adhesion	16	COL3A1, ITGA1, ITGA11, ACTN1, ITGB5, ITGA3, VTN, ITGB1, CTNNB1, THY1, CD44, ITGA6, ITGAV, ITGA7, RHOA, FN1	3.50	0.001613246
GOTERM_CC_FAT	GO:0005739	mitochondrion	208	PDP1, STOML2, IARS2, OGDH, HIBADH, GOT2, BAK1, AGPS, PDHA1, TMEM14C, PDPR, ACAA2, BSG, SUCLG2, SUCLG1, LYRM4, SYNJ2BP, BCL2L13, LETM1, NNT, PTRF, DLD, ATP5C1, MDH2, HSD17B10, ACADSB, TMX4, MTX1, SFXN3, SFXN1	3.16	4.81E-53

Category	GO term		Count	Genes	Fold Enrich-ment	Benjamini *P* value
				HSPA1A, ACAT1, HADHA, HADHB, COX6B1, ALDH4A1, FH, GPD2, MAOA, PHB, GARS, AFG3L2, VDAC2, VDAC3, PPA2, VDAC1, ATP5D, ATP5B, LONP1, P4HA1, SLC25A3, ATP5L, ATP5O, SLC25A1, ATP5I, DHTKD1, ATP5H, FUNDC2, NDUFB10, SLC25A4, ACO2, SLC25A5, AIFM1, SLC25A6, NDUFA13, CYB5A, CYB5B, DECR1, NDUFA10, NDUFA12, NDUFA11, TRAP1, CLIC4, TXN, TOMM22, APOOL, YWHAZ, ALDH18A1, ECH1, COX7A2L, ACSL1, MRPL12, PITRM1, ETFDH, HSD17B4, ACSL3, ETFB, ETFA, SHMT2, COX7A2, CS, SOD1, YWHAE, CPT1A, SOD2, SDHA, SDHB, TFRC, SDHC, SDHD, NLN, ATP5A1, TSPO, GRPEL1, COX5B, PDHB, FAHD1, UQCR10, CISD1, SLC25A24, LRRC59, TIMM9, DNAJC5, HADH, ALDH6A1, TMEM126A, COX6C, CLPP, LRPPRC, CAV2, CAV1, ME2, GLUD1, CTSA, PTRH2, MTCH2, GSTK1, HSPE1, ATP5J2, C21ORF33, AK3, ABCB6, IDH3A, SLC25A12, SLC25A11, USMG5, SLC25A13, TOMM70A, GLS, NDUFV1, NDUFV2, ALDH2, HSPD1, PC, UQCRC2, CYB5R3, CPT2, UQCRC1, CYC1, PRDX4, PRDX5, TIMM50, PRDX3, CLTC, UQCRFS1, UQCRQ, PRDX1, ACOT9, NDUFS7, TMEM173, NDUFS5, NDUFS4, NDUFS8, CAT, NDUFS3, ACAD9, NDUFS2, NDUFS1, SQRDL, SSBP1, CYCS, NDUFC2, TMEM70, COX4I1, TIMM22, LAP3, ACADVL, ALDH7A1, C1QBP, ALDH1B1, CTSD, CTSB, OAT, UQCRB, NDUFB3, NDUFB4, NDUFB8, NDUFB9, ETHE1, ECHS1, ALDH3A2, OXCT1, HSPA9, SCO1, NDUFA4, NDUFA5, DLST, NDUFA2, NDUFA8, PSAP, NDUFA9, ATP5F1, DPYSL2, PEX11B, HSDL2, PHB2, SCP2, MGST1		
GOTERM_ BP_FAT	GO:0030198	extracellular matrix organi-zation	16	RECK, COL3A1, HSD17B12, CST3, VTN, SERPINH1, ANXA2, EMILIN1, P4HA1, COL1A2, ACAN, COL6A2, COL12A1, LAMC1, COL1A1, ENG	3.00	0.007650404
GOTERM_ MF_FAT	GO:0019842	vitamin bind-ing	18	GC, SHMT2, SPTLC1, LEPREL2, OGDH, ALDH1L2, GOT2, MTHFS, LEPRE1, PLOD1, P4HA2, PLOD2, ALB, P4HA1, PLOD3, DHTKD1, OAT, PC	2.80	0.004239403

Category	GO term		Count	Genes	Fold Enrich-ment	Benjamini *P* value
GOTERM_ CC_FAT	GO:0031982	vesicle	102	A2M, VAPA, ATP1B3, APOA1, SND1, SLC2A1, RPN1, DNAJC5, RAB21, BSG, MYO6, ACTN4, ERP29, ACTN1, VAMP7, DLD, RAB14, VAMP2, ALDOA, CAV2, RAB7A, CAV1, ITGB1, CALU, STX12, SYPL1, ECE1, FGA, ALB, RAC1, TMED10, FN1, P4HB, GARS, ITGA1, LAMP1, LAMP2, PPIB, YIPF5, HSPD1, HSP90AB1, COPA, RAB5B, PDIA3, RAB5C, AP3S1, PDIA6, ANPEP, PDIA4, CLTC, PRDX1, CANX, SLC1A4, RABAC1, SLC1A5, COPB2, ATP6V0D1, TM9SF1, HSP90AA1, FLOT1, SLC3A2, MMP14, STOM, CLIC4, IGF2R, RAB5A, SORT1, CTSD, GNAS, CTSB, PROS1, COPE, TF, YWHAZ, GANAB, PF4, ANXA6, CD9, ANXA7, TMED2, TMEM33, RAB11B, SEC22B, RAB11A, HSPA5, SNAP23, THBS1, MYOF, HSPA8, RAB2A, YWHAB, ATP1A1, SPARC, SOD1, YWHAE, ANXA2, NCSTN, HSP90B1, LRP1, TFRC, ANXA11, ABCC4	2.51	6.88E-17
GOTERM_ BP_FAT	GO:0001944	vasculature development	29	RTN4, CAV1, NRP1, ATP5B, LEPR, COL3A1, CSPG4, ANPEP, CDH2, CTNNB1, BAK1, CD44, APOE, ITGAV, ERAP1, PLXND1, THBS1, PPAP2B, RECK, MYH9, MMP14, ANXA2, THY1, GPI, CDH13, ITGA7, COL1A2, COL1A1, ENG	2.25	0.003287588
GOTERM_ CC_FAT	GO:0005624	membrane fraction	109	HRAS, VAPA, VAPB, GNA11, CTNNB1, PGRMC1, LRRC59, SLC2A1, DDOST, RECK, DPAGT1, HLA-C, MOGS, HLA-B, POR, NME2, PTRF, RAB14, VAMP3, VAMP2, CAV2, TMX1, CAV1, GNAI2, DAG1, MME, ACP2, LMAN1, CALR, ITGB1, ECE1, RAC1, TMED10, ZMPSTE24, SCARB2, ERO1L, P4HB, CKAP4, SEC11A, ITGA1, EPHX1, VDAC3, LAMP1, LAMP2, ATP2A2, VCP, ITGA5, CD59, SPCS3, SPCS1, SPCS2, ENG, COPA, RAB5B, ATL1, LSS, CD151, LNPEP, HMOX2, SLC1A5, VKORC1, ATP6V0D1, KDELR1, NT5E, STS, AIFM1, FLOT2, FLOT1, CCDC47, KTN1, CYB5A, CYB5B, GNAQ, H6PD, IGF2R, RAB5A, SORT1, TOMM22, GNAS, DEGS1, CALD1, CTNND1, COMT, STT3A, ACSL1, TMED2, FMO3, SNAP23, PPAP2A, ACSL3, EHD2, PLP2, DLST, NCEH1, SLC12A4, ATP1A1, NPR3, CPT1A, SLC16A3, NCSTN, MGST3, HSP90B1, LRP1, ABCC3, DPM1, ABCC4, ABCC1, MGST1, SSR3, SPTAN1	2.22	3.56E-14

Supplementary Table 4. List of 473 proteins shared between devitalized ECM and human bone samples. Protein IDs are ranked for abundance in devitalized ECM (LFQ values).

P63261	Q01995	P60903	C9JA28	E9PMR4
P07355	Q00325-2	P13073	Q02218	P02786
CON__P02769	P49755	Q96AG4	P56134-3	P08238
P04264	P23284	P31930	Q6YHK3	C9J3L8
P15144	P40926	P07339	P63104	I3L1P8
P08133	P04406	P21589	P04179-4	P46977
P08758	P38646	P09382	P10301	Q13724-2
CON__P12763	P00367	Q15363	P55084-2	Q9NRP0
P13645	P24821-4	P00403	Q71U36-2	O60831
P06576	P02452	H0YD13	P08123	P30040
Q14195	P12236	Q8IWA5-3	B4E2V5	Q5JP53
P35908	P43121	P12111-2	Q15165-3	Q9Y2Q3
P14625	Q9BVK6	P05186	P00167-2	P08574
P11021	P39656	P45880	H0YNG3	K7EJE8
P35527	Q9Y6N5	Q9BVC6	B4DJV2	Q969X5-2
P00387-2	P02545-2	Q9Y4L1	Q969H8	P61009
P04083	CON__Q3SX09	P00338	P13667	P05141
P35579	Q13423	Q12907	Q9Y3B3-2	Q9UJS0
P25705	P51571	J3KNF8	Q9NVJ2	P05388
P68032	P02751-17	P61106	Q99714	Q9NYL4-2
P27824	O43707	P14314-2	P09622	P24752
P04843	P36269	P55072	O75947	CON__Q2KIS7
P21333-2	Q14108	Q6NZI2	P31040	P21912
P08670	Q07065	P04040	Q99623	P30044-2
Q09666	Q6DD88	P30447	P60981	O75489
G5EA52	P06733	P51572	E9PR44	Q12797-10
P12814	P23634-7	P61026	P30084	P04075
P05556	P21964-2	Q9BTV4	P07954-2	B4DT77
CON__P15497	P61224	Q9NYU2-2	Q01628	Q9BS26
Q9NZM1-6	P18084	B4DMK0	Q13162	Q00765
P10809	O75396	O15260-2	Q92743	Q14165
P27797	P30048-2	Q53GQ0	P13611-2	P67936
P50454	Q9UBI6	P47985	P36957	P30049
P04844	P16615-5	Q5JPE7-2	E7ETY7	P62820
E9PJK1	P11142	O95202	Q9H9B4	P12109
P56199	P61019	O95831-3	Q9BSJ8	P07942
P21796	F8W1R7	P50995-2	P26038	Q16563-2
Q03135	P23528	P62937	Q86UY0	J3KTF8
P06756-3	Q9H0U4	P19105	B7Z6B8	P13647
P06396-2	O75915	P35232	P62258	P11177-2
P07237	P62873	Q99715-4	P52907	O43852
Q14697	P51149	Q9BWM7	CON__P17690	P54289-4
Q9NQC3-2	Q9Y490	P28331-4	B4E2S7	CON__Q3ZBS7
Q9UBG0	P09525	P51659	P11047	Q99536
CON__ENSEMBL:ENS-BTAP00000024146	P49257	P51148	Q96JJ7	A6NNI4
	P04899	Q99798	P07996	P61981
Q07954	Q15084-3	O15173	Q32P28	P39019
Q08431	P22695	P30050	P84077	O95197-3
P07099	P24539	J3QS39	Q00610-2	Q06830
CON__Q0IIK2	P18206-2	P54709	Q05682-5	P49419-2
E9PNW4	P09493-3	CON__ENSEMBL:ENS-BTAP00000016046	P29992	Q9H3N1
Q9UHG3	P31949		P07737	P54920
Q14764	P48047	Q15758	Q15005	Q01082
P04792	P20340-2	P10620	P07951-2	Q7Z7H5-3
P40939	P49748-2	Q15836	Q6NUK1	P05091

E9PEP6
Q92896
P63000
P61586
P31946-2
P00505
F8VQX6
Q13011
P53007
O60762
B4DL14
Q9Y3A6
P43304-2
Q9BQB6-3
P46783
P11233
P59998
P02533
O15031
P16435
Q9Y394-2
Q07021
P60953
Q969V3-2
Q96I99
P46940
O14735-3
Q8N0U8
Q9UIJ7
P11717
Q96HE7
P21397
P09486
P50148
P51636-2
Q9UFN0
O00469
J3QS48
Q9UBV2
P62913-2
CON__Q2KJF1
P09211
Q9Y3E5
P38117
P62269
P22314
P47756-2
J3KN67
P62879
Q13813-3
P62736
O14880
P55809
P01112
P40261
Q969G5
E5RI99
Q14699
E7EMM4
Q53TN4-3
P06744
Q04917
CON__ENSEMBL:ENS-
BTAP00000007350
H0YL12
K7ERI7
P05387
Q9UJZ1-2
P63092-3
Q86UE4
P18669
O75369-2
E9PN66
F8W031
P07858
P42765
M0QZN2
P11234
P19404
P12235
P04632
X6RJP6
P61421
P27348
Q96A33-2
Q9NS69
O00264
P13639
P12110-3
P61158
H3BN98
P07900
O15144
P23396
P00558
CON__Q3SZV7
E9PH64
Q86Y82
O15400-2
Q9NZN4
Q9Y6C2
Q8N1B9
P62081
O95479
P30483
P07602
E9PNJ4
P62750
B4DJA5
Q8N5K1
O96000
P48449-2
P00441
P30038
Q8NBX0
P10321
Q9NP72
Q16555
P31937
P16112-2
Q01518-2
P47755
P24844
P18085
C9JFR7
P08559-3
P10599
P11166
Q96S97
Q9Y277
E7EQU2
G3V1B6
Q02252-2
P62906
P62851
P61160
O14494
Q08257-3
E5RHW4
P57105
O75306-2
Q86UP2-2
H7BZ81
Q16836
P32969
Q9NR31
P38919
P61006
Q8WY22
Q9NZ01
J3QRD1
Q6YN16
P62834
CON__Q03247
E7EPM6
Q14254
P60866
Q15293
CON__Q3Y5Z3
Q13683-9
P53597
E9PIE4
H3BR27
Q13636
Q9H2U2-6
Q4KMQ2-3
Q9UBS4
P49821-2
F5H0J3
Q9Y696
O75955
CON__P07224
P28066
P10619-2
Q15404-2
P61020
CON__Q3T052
P50395
Q6P587
Q96CG8-3
P23229-4
Q92629-3
O43181
REV__CON__P02672
Q9BWH2
Q9H1E5
P81605
Q5JX45
Q9H0U3
C9JGJ9
P84095
B4DQ51
Q14739
P28838-2
F5H261
Q96QK1
P06748-2
F5H5N1
B5MCE2
P08473
Q9NZ08